Available online at www.sciencedirect.com
SCIENCE DIRECT
Journal of Colloid and Interface Science 288 (2005) 155–165
JOURNAL OF Colloid and Interface Science
www.elsevier.com/locate/jcis

Phase behavior of block co-poly(ethylene oxide–butylene oxide), $E_{18}B_9$ in water, by small angle neutron scattering ☆

Alexander I. Norman [a,*], Derek L. Ho [b,c], Alamgir Karim [a], Eric J. Amis [a]

[a] *Polymers Division, Stop 8542, National Institute of Standards and Technology, 100 Bureau Drive, Gaithersburg, MD 20899-8542, USA*
[b] *Center for Neutron Research, Stop 8562, National Institute of Standards and Technology, 100 Bureau Drive, Gaithersburg, MD 20899-8562, USA*
[c] *The University of Maryland, College Park, MD 20742, USA*

Received 20 December 2004; accepted 23 February 2005

Available online 31 March 2005

Abstract

We present a small angle neutron scattering (SANS) study into the micellar structures of diblock copolymer $E_{18}B_9$ (where E denotes a ethylene oxide unit and B denotes a butylene oxide unit, 18 and 9 being the number of repeat units respectively) in aqueous solution over a range of five different concentrations (0.2, 1.0, 10.0, 20.0, and 40.0% (by mass fraction)) and eight temperatures (10 to 90 °C). The NG7 30 m SANS instrument provides a q range of 0.0009 to 0.5548 $Å^{-1}$, thus probing the structure over a very broad length scale. At low temperature and low concentration, spherical micelles exist, elongating into worm-like structures at higher temperatures. This transition is observed by the scaling of the scattered intensity at low q and confirmed upon fitting to an appropriate model. Upon increasing concentration, the micelles pack into ordered arrays of either hexagonally packed rod-like micelles or lamellar sheets, again dependent on temperature. Both concentration and temperature effects of this block copolymer have been discussed.

Keywords: Micelles; SANS; Block copolymers; PDDF; Aqueous

1. Introduction

Over the last decade the micellization and gelation of many poly(oxyalkylene) block copolymers have been studied in great depth and are well documented [1]. In industry, such materials possess many desirable properties and are used widely [2], for example, in oil extraction, burn wound dressings, personal care products, as well as biologically [3], e.g., in bile salts that act as surfactants for the digestion of fats in the body.

E_nP_m block copolymers—where P represents a propylene oxide block, E represents an ethylene oxide block and n and m represent the number of repeat units—have been available for a number of years over a wide range of chain lengths and composition [4]. In 1955 the Wyandotte Chemicals Corporation disclosed the development of the production of ethylene oxide (E)–butylene oxide (B) block copolymers [5]. Commercial introduction of these samples was delayed until 1993 when diblock (E_nB_m) and triblock ($E_nB_mE_n$) copolymers were first marketed by the Dow Chemical Company [6].

Evidence for changes in micelle shape comes from the phase transitions observed by many poly(ethylene oxide)–poly(butylene oxide) block copolymers in aqueous solution, such as the body-centered-cubic (BCC) to hexagonal transition that occurs for $E_{16}B_{10}E_{16}$ [7]. The techniques that elucidate such information include polarized light microscopy, rheology, small angle X-ray scattering (SAXS) and small angle neutron scattering (SANS).

A considerable body of work has been carried out on block copolymers in solution via time resolved scattering

☆ Official contribution of the National Institute of Standards and Technology; not subject to copyright in the United States.

* Corresponding author. Present address: Department of Chemistry and Biochemistry, University of Maryland, College Park, MD 20742-2111, USA.
E-mail address: anorman1@umd.edu (A.I. Norman).

0021-9797/$ – see front matter
doi:10.1016/j.jcis.2005.02.091

techniques (SAXS and SANS) [7–13]. This is a reliable way of determining the mesophase morphology and has been carried out by Fairclough and co-workers [8] for the diblock copolymer $E_{41}B_8$, where a phase diagram was constructed by SAXS measurements that displayed strong agreement with rheological data. It was found that in a region between 24 and 28% (by mass fraction) polymer existed where both face-centered and body-centered cubic structures were observed depending on the temperature. Upon increasing concentration, phase transitions from a BCC phase to hexagonally packed cylinders to lamellae were evident. This has been observed for many block copolymers in many solutions and has been explained in terms of molecular packing and interfacial curvature [14]. Phase transitions of this type are of great interest which will become apparent in this study.

Many publications in the literature [15–17] describe the shape transition within micelles, notably the spherical to elongated micelle transition on increasing temperature, which is of considerable interest to this work. King et al. [15] describe the spherical to rod-like micelle transition at 62 °C for a 1% (by mass fraction) sample of Synperonic P85 ($E_{25}P_{40}E_{25}$), whereas Mortensen et al. [16] modeled the same polymer SANS data to a prolate ellipsoid. As the temperature of the system is increased, the micelles become larger until a characteristic temperature is reached, where the micelle size approaches the size of a fully stretched propylene oxide chain. The micellar structure therefore changes and becomes markedly non-spherical [17].

The process of micellization is entropically driven as stated by Soni et al. [18]. The same block copolymer (Dow notation BM45) was used by Soni as is used in this paper (but of a different batch). SANS was carried out on solutions from 1 to 10% (by mass fraction of polymer) at 30 °C. Micelles were spherical at such temperatures and over the concentration region were of a constant radius (core radius measured at 43 Å). The effect of temperature was explored for a 2% solution. On increasing temperature to 50 °C, a transition from a spherical to ellipsoidal micelle was observed, accompanied by significant changes in micelle size (prolate ellipsoid of dimension 37 × 136 Å) and association number ($N = 318$ for spheres and $N = 743$ for ellipsoids). This effect was attributed to the dehydration of the hydrophilic blocks at elevated temperatures.

The elongation of spherical micelles of ethylene oxide–butylene oxide systems has also been observed by Chaibundit et al. [19,20]. Micellization of $E_{11}B_8$ in water [19] was observed by dynamic light scattering: hydrodynamic radii were obtained at 30 °C (∼60 Å) and 40 °C (∼80–140 Å). The increase in radius also brought about an increase in association number ($N = 63$ at 25 °C and $N = 339$ at 40 °C), characteristic of micelle elongation. The solubilization capacity for drugs (such as Griseofulvin) of such elongated micelles was greater than of spherical micelles. Chaibundit et al. also describe the mesophase behavior and the relation to the spherical and to elongated micelle transition [20]. The diblock copolymer $E_{17}B_{12}$ was shown, by dynamic light scattering, to form elongated micelles. On increasing polymer concentration to 5 wt%, a low modulus gel was observed (at 37 °C). Hard gels were shown to be predominant in concentrations exceeding 25 wt%. Such structures displayed rich rheological properties. Rheology and polarized light microscopy were used to estimate the mesophase morphology. A birefringent gel, attributed to grains of elongated aligned micelles, was observed at room temperature for such hard gels. High temperature gels were also shown to persist at temperatures exceeding 70 °C. Such gels were shown to be isotropic by polarized light microscopy. Rheology measured a storage modulus exceeding 1 kPa. It was speculated that this phase was of an ordered cubic structure. The formation of such a phase was reportedly due to scission of cylindrical micelles at elevated temperatures.

Recently, Hamley et al. [21] confirmed the transition between spherical and elongated micelles in a 1% solution (by mass fraction) of diblock copolymer $E_{18}B_{10}$. This was performed via SANS techniques over a temperature range 20–60 °C. This is consistent with the observation of hexagonally packed rod-like micelles for the same block copolymer in more concentrated solution [22].

In this work, the technique of SANS is used to explore this phenomenon in the same block copolymer. The block copolymer, available from Dow Chemicals and denoted BM45-1600, is from a separate batch and of architecture $E_{18}B_9$. Small differences in composition will occur from batch to batch but as one would expect, since the B block is only one unit shorter, the behavior in aqueous solution should prove to be remarkably similar. Existing work shows the elongation of such micelle structures. We attempt to reproduce such s phenomenon and further prove, not only by SANS data alone, but also by performing an inverse Fourier transformation on the SANS data, to yield the pair distance distribution function, $p(r)$. Our SANS data is recorded over a wider concentration and temperature window, therefore consequences of micelle elongation on the mesophase formation are investigated. As described in the experimental section, SANS data is collected over a broader q range than that described by Hamley et al. [21], thus gaining insight into information at larger length scales.

2. Materials and methods

2.1. Synthesis and characterization of polymers

The diblock copolymer $E_{18}B_9$ was obtained as a gift from Dow Chemicals and was given the notation BM45-1600. To compare the results with previous studies on this polymer, the material was used as received and not purified further. Other batches used of this same material have been quoted as $E_{18}B_{10}$ [21] and $E_{17}B_{12}$ [20]. Such materials are synthesized by sequential anionic polymerization of 1,2-butylene oxide and ethylene oxide. Further details of the synthesis of similar diblock copolymers (such as E_6B_{11}, which forms multil-

amellar vesicles in aqueous solution) have been described elsewhere [23]. The composition was determined by nuclear magnetic resonance (NMR) spectroscopy using methods described previously [24].

2.2. Micelle preparation

Neat block copolymer was added to deuterated water, D_2O, until the desired concentration was reached. The sample vial was shaken by hand for approximately 60 s. Aqueous dispersions were prepared in 0.2, 1.0, 10.0, 20.0, and 40.0% by mass fraction concentrations. Samples were allowed to stand for a minimum of 48 h before any analysis was performed.

2.3. Small angle neutron scattering measurements

SANS experiments over the q range from 0.0009 to 0.5548 Å^{-1} were carried out using the NG7 30-m SANS instrument at the National Institute of Standards and Technology (NIST) Center for Neutron Research (NCNR), Gaithersburg, MD [25].

Three instrumental settings were used to cover the range of the scattering vector, q, where $q = (4\pi \sin\theta)/\lambda$, 2θ being the scattering angle and λ the neutron wavelength. The three settings (wavelength and sample-to-detector distance) used to achieve this q range are 8.09 Å and 15.3 m (with the focusing lens configuration [26]), 6.0 Å and 6.0 m, and 6.0 Å and 1.1 m with a wavelength resolution of $\Delta\lambda/\lambda = 0.11$. The scattered intensity was corrected for background and parasitic scattering, placed on an absolute level using a calibrated secondary standard and circularly averaged to yield the scattered intensity, $I(q)$, as a function of the wave vector, q. Finally the low incoherent background scattering was estimated. This was determined from the asymptotic slopes of $I(q)q^4$ vs q^4 [27] and subtracted from each data set.

The samples were dissolved in D_2O to provide a low incoherent background and strong contrast. Samples were loaded into quartz cells of 1 mm path length. The five samples prepared were investigated at temperatures of 10, 20, 30, 40, 50, 65, 80, and 90 °C. Due to time constraints not all samples were probed at such a low q range, giving a q range of 0.0053 to 0.5548 Å^{-1} for some of the samples studied. Table 1 lists each the temperature and the q range studied for each concentration of block copolymer. The low concentration samples (0.2 and 1.0%) were at such a concentration where structure factor effects can be neglected and the SANS experiment probes the single particle form factor which is a function describing the shape of the non-interacting individual micelles. This is discussed in greater detail in the proceeding section. Samples at higher concentration (10.0, 20.0 and 40.0%) were studied to observe the possibility of the formation of lyotropic liquid crystalline phases. The error (standard uncertainty) associated with the SANS experiments is dependent on various factors, such as the detector count rate, the estimation in conversion of pixel number to scattering vector, and the secondary standard. For clarification purposes, the error bars in some of the figures have been omitted.

Table 1
Temperature and q range investigated for each block copolymer concentration

Concentration (wt%)	Temperature (°C)	q range (Å^{-1})
0.2	10–40, 65, 90	$0.0065 \leqslant q \leqslant 0.5548$
	50, 80	$0.0009 \leqslant q \leqslant 0.5548$
1.0	10, 30, 50, 80	$0.0009 \leqslant q \leqslant 0.5548$
	20, 40, 65, 90	$0.0065 \leqslant q \leqslant 0.5548$
10	10–90	$0.0065 \leqslant q \leqslant 0.5548$
20	10–90	$0.0065 \leqslant q \leqslant 0.5548$
40	10, 30, 50, 80	$0.0009 \leqslant q \leqslant 0.5548$
	20, 40, 65, 90	$0.0065 \leqslant q \leqslant 0.5548$

3. Theory and data analysis

For a system of particles the scattered intensity is given as

$$I(q) = n\Delta\rho^2 V^2 P(q) S(q), \tag{1}$$

where n is the number density of the particles, $\Delta\rho$ is the difference in scattering length density, V is the volume of particles, $P(q)$ is the form factor, and $S(q)$ is the structure factor, with the wavenumber, $q = (4\pi \sin\theta)/\lambda$ (θ is the angle between the scattered and incident beam and λ is the wavelength of the incident radiation).

The form factor is a function which describes the intra-particle scattering from the *shape* of the scattering particles. The structure factor is a function which describes the inter-particle scattering due to the *interactions* of the scattering particles. The spatial correlations arising in the structure factor are due to the radial distribution function, $g(r)$, which is related to the probability of finding the center of any particle at a distance r from the center of a given particle. For N particles in a volume V at a distance r from any given particle, the structure factor is defined as [29]

$$S(q) = 1 + 4\pi \frac{N}{V} \int_0^\infty \big[g(r) - 1\big] r^2 \frac{\sin(qr)}{qr}\, \mathrm{d}r. \tag{2}$$

The structure factor, $S(q)$, given in Eq. (2) is neglected in many data sets throughout this paper since the concentration is extremely low, hence $I(q)$ follows the form factor which was modeled depending on the *shape* of the scattered particles, described below.

3.1. Micelle shape analysis

We can understand the SANS profiles, such as that illustrated in Fig. 1, of such systems by concentrating on three separate regions. At low q, the behavior of $I(q)$ is general and independent of the shape of the scattering particle. This

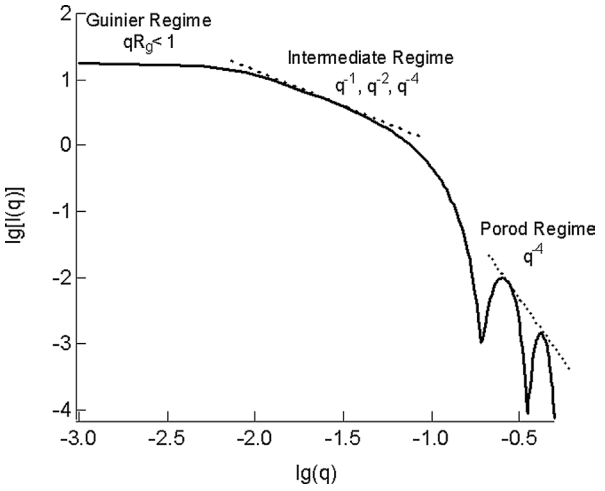

Fig. 1. Generalized small angle scattering profile showing the different regimes which reflect different decays of intensity in scattering vector, q.

is because at small q values ($qR_g \leqslant 1$) the spatial resolution is not sufficient to elucidate particle shape and only information regarding dimension can be obtained. In this case $I(q)$ is described by the Guinier relation [28]

$$I(q) = I(0)\exp\{-q^2R_g^2/3\}, \tag{3}$$

where R_g is the radius of gyration of the particle and $I(0)$ is the scattered intensity at $q = 0$, which is determined from the double logarithm plot:

$$\ln[I(q)] = \ln[I(0)] - \frac{q^2R_g^2}{3}. \tag{4}$$

Since the data shown is in absolute scale, $I(q)$ being expressed in units of cm^{-1}, we can make use of $I(0)$, which is calculated by the y-intercept of a Guinier plot as expressed in Eq. (4), to determine the aggregation number, which is defined as the number of molecules that are within the micelle. The aggregation number, n_{agg}, is determined from

$$I(0) = n_{\mathrm{agg}}\phi_{\mathrm{polymer}}K_nV_i, \tag{5}$$

where the neutron contrast factor $K_n = \Delta\rho^2N_A$ and $\Delta\rho = \rho_i - \rho_j = (b_i/v_i - b_j/v_j)$. N_A is Avogadro's constant (6.023×10^{23} molecules/mol), ϕ_{polymer} is the concentration of polymer, V_i is the specific volume of species i in units of cm^3/mol, and $\Delta\rho^2$ is the square of the difference in scattering length density ($\mathrm{mol}^2/\mathrm{cm}^4$) between polymer ($i$) and solvent ($j$). b is defined as the scattering length in cm.

The high q region of the SANS profile describes the Porod regime where the spatial resolution is very good. This enables the observation of the interface between particle and solvent. Here, the intensity typically scales as q^{-4} [29]. Polydispersity in the size and the shape of the scattered particles will affect this scaling due to a broader interface between scattered particles and surrounding solvent.

The intermediate range of the profile is the region in which the form factor contains information regarding particle size and shape. In this region the scaling of $I(q)$ results from the dimensionality of the scattered particle, for example, the scattered intensity of a rod-like micelle scales as q^{-1}, whereas a vesicle shell or a disk scales as q^{-2} [30].

Further micelle shape determination is achieved using the generalized indirect Fourier transformation (GIFT) method [31]. The conventional Fourier transformation of $I(q)$ involves the integral

$$p(r) = \frac{1}{2\pi^2}\int_0^\infty I(q)qr\sin(qr)\,\mathrm{d}q, \tag{6}$$

which yields the pair distance distribution function $p(r)$, where r is the distance in real space. This function can be used to determine size, shape and internal structure of scattered particles with high accuracy in the size range of approximately 10 to 1000 Å (depending on the q range of the instrument used to collect the data). The $p(r)$ function can be understood as follows. The scattered particle is divided into many small volume elements (small in comparison to local density fluctuations). The $p(r)$ function is proportional to the product of the different scattering lengths n_in_k of two volume elements i and k with a center-to-center distance between r and $r + \mathrm{d}r$. Similarly, the height of the $p(r)$ function is proportional to the number of such scattering lengths that are found inside the particle within the interval r to $r + \mathrm{d}r$ [31]. The direct calculation of $p(r)$ using Eq. (6) requires scattering data in the full q range from 0 to ∞. The limited q range available experimentally will lead to strong oscillations in $p(r)$. These effects have been minimized in a new data analysis technique using the indirect Fourier transformation [31–33]. This method performs desmearing and Fourier transformation simultaneously, assuming that $p(r) = 0$ for $r > D_{\max}$, where $D_{\max}$ is the maximum particle dimension.

The form factor arising from the scattering of monodisperse, non-interacting hard spheres is shown in the equation [31]

$$P(q) = \left\{\frac{3[\sin(qR) - qR\cos(qR)]}{(qR)^3}\right\}^2, \tag{7}$$

where R is the radius of the scattered particle.

Fig. 2 shows our SANS data with the respective fit to Eq. (7) for 0.2 and 1.0% at 10 °C.

The non-interacting spherical model (which does not take into account polydispersity) fits the data well over the q range probed. The oscillations at higher q values are smeared out due to polydispersity effects. The scaling of $I(q)$ at low q is q^0, describing the Guinier region of the curve, indicating that no large particles are present, such as worm-like micelles that may possibly mask the Guinier region at the lowest accessible q range, or any inter-particle interactions arising from $S(q)$ contributions. The radii obtained were 58.0 ± 1 Å for 0.2%. Fig. 2 also shows the SANS data and the fit to a spherical model for 1%. The significant upturn in $I(q)$ at low q is over a q range lower than that probed for the data shown for 0.2%. The fit to the spherical

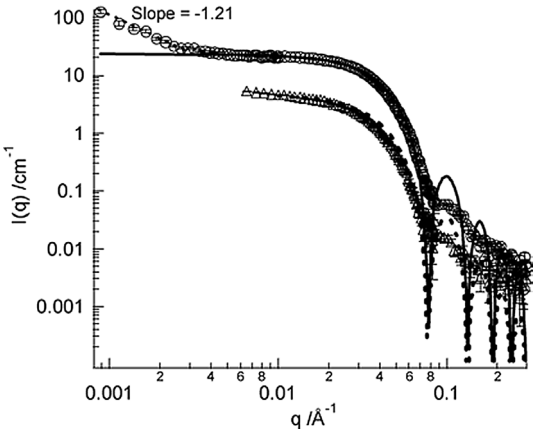

Fig. 2. SANS intensity profiles, with respective fits to a monodisperse non-interacting sphere, for 0.2% by mass fraction (open triangles, data; solid line, fit) and 1.0% by mass fraction (open circles, data; broken line, fit) $EO_{18}BO_9$ in D_2O at 10 °C. The lines show the fit to Eq. (3); a hard sphere model with no polydispersity.

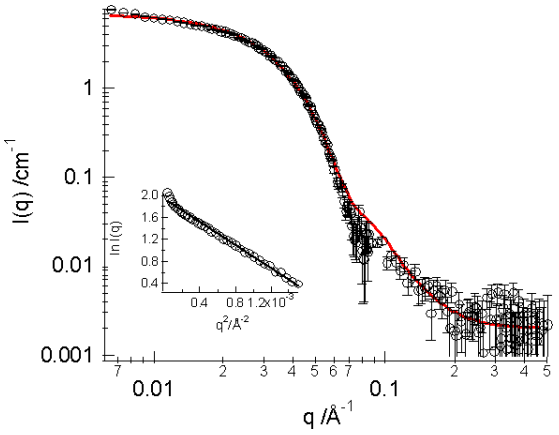

Fig. 3. SANS intensity profiles from a solution of 0.2% by mass fraction of $EO_{18}BO_9$ at 20 °C. The solid line indicates the fit to a hard sphere with polydispersity. Inset shows the Guinier plot, $\ln q = \ln[I(0)] - q^2 R_g^2/3$, where $y = 1.9266 - 1045x$.

model works well for 1% over the same q range as that for 0.2%. This model also yields a radius of 58.0 ± 1 Å for 1.0%. The change in slope at very low q ($I(q)$ scales as $q^{-1.21}$ rather than zero) observed for 1.0% may be attributed to a weak interaction of micelles that have formed an aggregate which is beyond the size range detectable by the conventional SANS setup.

The introduction of polydispersity into this model is illustrated in Fig. 3, which shows SANS data and the respective fit for a 0.2% polymer solution at 20 °C. The monodisperse model was used in Fig. 2 for illustrative purposes only, data was fitted using the polydisperse model, and the same R value was obtained (which is summarized in Table 2). This function [31] calculates the scattered intensity for a population of polydisperse spheres including hard sphere interactions between the particles. A Schultz distribution [34] is used to describe the polydispersity, p, of the diameter, $p = s/R$, where s^2 is the variance of the distribution and R is

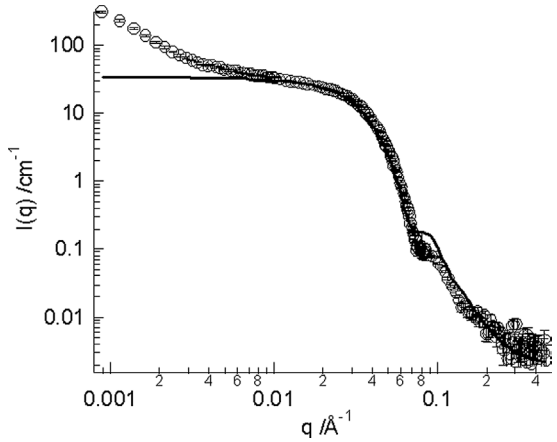

Fig. 4. SANS intensity profile from a solution of 1.0% by mass fraction of $EO_{18}BO_9$ at 50 °C. The solid line indicates the fit to the model describing polydisperse hard spheres.

the mean particle radius. We can see how the introduction of polydispersity smears out the high q oscillations in $P(q)$ by comparing Figs. 2 and 3. At low temperatures the intensity, $I(q)$, scales as $q^{-0.4}$ over the q range 0.007 to 0.02 Å^{-1}. This deviation from the Guinier regime has been attributed to polydispersity in size of scattering elements. However, other possible explanations are the elongation of the spherical particles into oblate or prolate ellipsoids. In this study the fit to a polydisperse spherical model proved more accurate than the fit for an ellipsoid. The inset to Fig. 3 shows the Guinier plot, which is performed to extract $I(0)$ which is used, in our case to determine the aggregation number.

The effect of increasing the concentration five-fold, to 1 wt% polymer at 20 °C, is shown in Fig. 4. The fit to a polydisperse hard sphere gives a radius of 54 ± 1 Å with a polydispersity of 15%. Once again, we see the deviation from the scaling of q^0 in intensity at the lowest q range, which we assume is due to aggregation effects as described above.

The second model we shall discuss is that of a prolate ellipsoid. A prolate ellipsoid is needle-like in shape, as opposed to an oblate ellipsoid, which is disk-like and has a very different scattering profile. For the prolate ellipsoid the form factor is described [35],

$$P(q) = \int_0^1 f^2\left[qr_b\left\{1 + x^2(\nu^2 - 1)\right\}^{1/2}\right] \mathrm{d}x, \tag{8}$$

$$f(z) = 3V_{\mathrm{ell}} \frac{(\sin z - z\cos z)}{z^3}, \tag{9}$$

$$V_{\mathrm{ell}} = \frac{4}{3}\pi r_a r_b^2, \qquad \nu = \frac{r_a}{r_b}, \tag{10}$$

where $f(z)$ is the scattering amplitude and $z = qr_b\{1 + x^2(\nu^2 - 1)\}^{1/2}$, r_a is the short axis of the ellipsoid, r_b is the long axis, ν is the ratio of the short axis to the long axis, $x = R_g^2 q^2$ (R_g is the radius of gyration), and V is the volume of the ellipsoid.

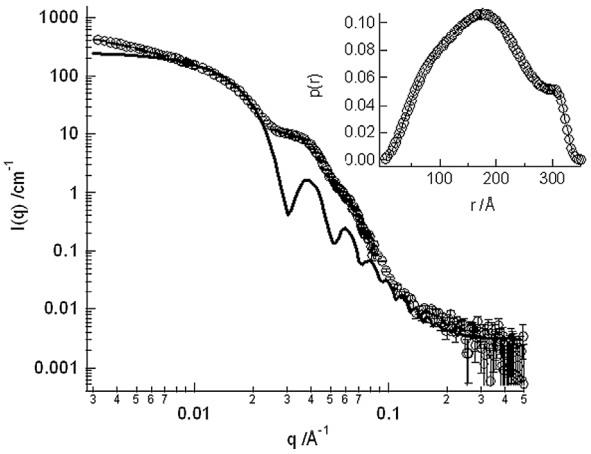

Fig. 5. SANS intensity profile from a solution of 1.0% by mass fraction of $EO_{18}BO_9$ at 50 °C. The solid line indicates the fit to a prolate ellipsoid. The inset shows the pair distance distribution function.

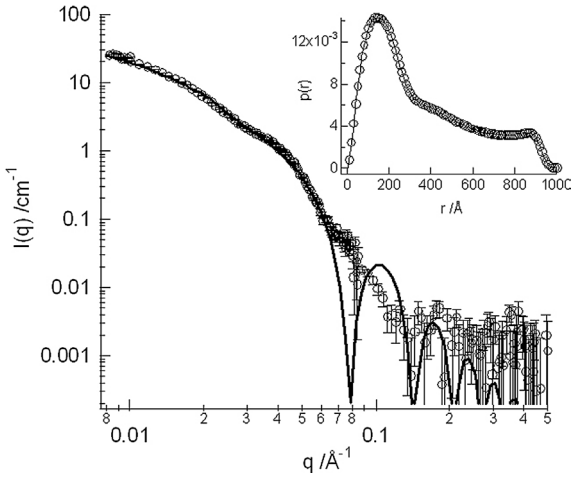

Fig. 6. SANS intensity profile from a solution of 0.2% by mass fraction of $EO_{18}BO_9$ at 50 °C. The solid line indicates the fit to a semi-flexible chain with excluded volume. The inset shows the pair distance distribution function.

On increasing temperature, the observation of an increased aggregation number is evident (we refer the reader to Table 2 for a summary of all data) along with the upturn in $I(q)$ at low q, suggesting the elongation of these spherical micelles into elongated structures. Fig. 5 shows the SANS data for 1.0 wt% polymer at 50 °C and the fit to the model for a prolate ellipsoid. Polydispersity effects are not included in this model, which explains why the oscillations at larger q values are so well defined in comparison to the data. A broad peak observed at 0.045 $Å^{-1}$ arises from form factor contributions due to the micellar radius. The model gives a long axis of 250 ± 10 Å and a short axis of 130 ± 10 Å. The inset to Fig. 5 displays the $p(r)$. This function is not perfectly symmetric and is characteristic of an elongated structure.

Finally, a model for semi-flexible chains with excluded volume [36] is fitted to the data which describes non-rigid, elongated micelles, which we will refer to as "worm-like" micelles. Such structures can be estimated from the scaling of $I(q)$ at low q. The scattered intensity observed in this system scales as $q^{-5/3}$ [36], which is intermediate of the scaling law for rigid rods (q^{-1}) and Gaussian coils (q^{-2}). This suggests that the micelles are not rigid; they do possess some flexibility and are worm-like in shape.

The worm-like model, which is a non-linear least squares fit of the scattered intensity for semi-flexible chains with excluded volume, can be described as the following. Consider a polymer of N units. When diluted in a solvent the polymer gets entangled as a result of the chain flexibility. The motion of the chains can be modeled by the random walk model [36] that describes the features of the polymer configurations and diffusive motion. The length of such a walk is given as $\langle R^2 \rangle = aN^{1/2}$, where a is a given length. In good solvents (such as water for polymers in this study), the polymer coil behaves as a self-avoiding random walk (the walk has an additional restriction in that it cannot cross itself within a given distance, a). This concept is known as the excluded volume effect and is a part of the worm-like micelle model used in these subsequent calculations. The Kuhn length, b, which is considered as rigid segments behaving independently over the whole chain, can characterize the stiffness of the chain. Hence in a semi-flexible chain of contour length, L, there are L/b segments. Values of the Kuhn length appear in the intermediate region of the SANS curve that can be used to describe the chain flexibility. Further details of this model can be found in Pedersen and Schurtenberger [36] and references therein. Further evidence to suggest this worm-like shape comes from the pair distance distribution function, PDDF, or $p(r)$.

An example of a fit to this model is shown in Fig. 6. Fig. 6 shows the SANS data at 50 °C for 0.2 wt% polymer. The model gives fitted parameters, $R = 49 \pm 1$ Å, $b = 145 \pm 10$ Å, and $L = 950 \pm 10$ Å. The inset displays the $p(r)$ function. This is typical of elongated structures due to the asymmetry shown. Ripples appearing at larger values of r are characteristic of axial inhomogeneity along the cylinder, which is present if such structures, and possess some degree of flexibility. The point at which the $p(r)$ falls to zero is indicative of the particles maximum dimension, which is 1000 Å, in good agreement with the fit to the worm-like model in $I(q)$. Such transitions observed from spherical to ellipsoidal to "worm-like" micelles will be discussed in the next section.

The subsequent fitted parameters for 0.2 and 1.0 wt% (at all temperatures investigated) are shown in Table 2 for all models used.

3.2. Consequences of micelle shape on mesophase behavior

The structure factor, $S(q)$, is a relevant parameter to the observed scattered intensity as the concentration increases to 10 wt%. Correlation peaks shown in $I(q)$ are apparent, indicating the ordering of micelles into lyotropic liquid crystalline phases.

Table 2
Fitted parameters for 0.2 and 1.0% by mass fraction of $EO_{18}BO_9$ in D_2O over a range of temperatures

Concentration (wt%)	T (°C)	Model	Parameters	N_{agg}	Polydispersity
0.2	10	PDHS	$R = 53$ Å	37	0.20
0.2	20	PDHS	$R = 57$ Å	51	0.22
0.2	30	PDHS	$R = 58$ Å	54	0.20
0.2	40	PDHS	$R = 60$ Å	58	0.20
0.2	50	Worm-like	$R = 49$ Å, $b = 145$ Å, $L = 950$ Å	334	–
1.0	10	PDHS	$R = 54$ Å	35	0.15
1.0	20	PDHS	$R = 58$ Å	46	0.15
1.0	30	PDHS	$R = 60$ Å	54	0.15
1.0	40	PDHS	$R = 62$ Å	59	0.17
1.0	50	Ellipsoid	$R_{short} = 130$ Å, $R_{long} = 160$ Å	371	–
1.0	65	Ellipsoid	$R_{short} = 135$ Å, $R_{long} = 180$ Å	–	–
1.0	80	Ellipsoid	$R_{short} = 135$ Å, $R_{long} = 200$ Å	–	–
1.0	90	Worm-like	$R = 42$ Å, $b = 100$ Å, $L = 1500$ Å	–	–

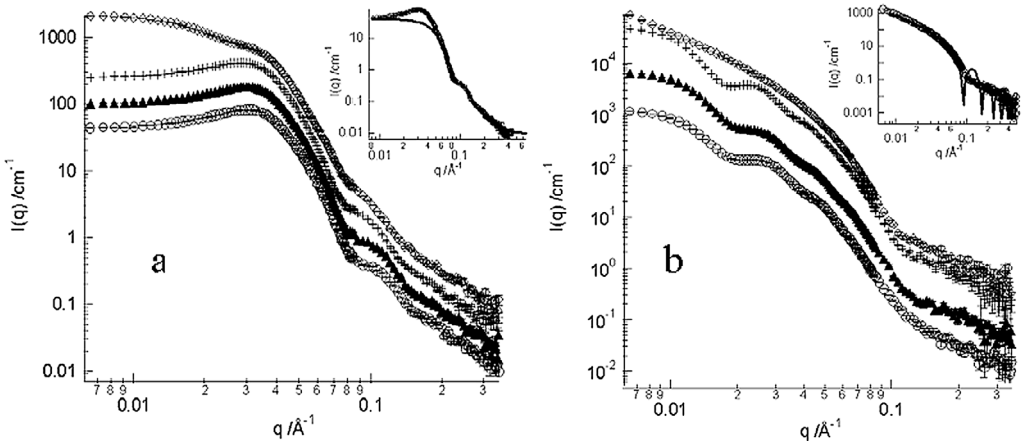

Fig. 7. SANS intensity profiles from a solution of 10% by mass fraction of $EO_{18}BO_9$ at (a) lower temperatures (open circles, 10 °C; filled triangles, 20 °C; crosses, 30 °C; open diamonds, 40 °C; inset displays the fit to the data at 10 °C to a polydisperse hard sphere model) and (b) higher temperatures (open circles, 50 °C; filled triangles, 65 °C; crosses, 80 °C; open diamonds, 90 °C; inset displays fit to the data at 90 °C to a semi-flexible chain with excluded volume).

Figs. 7a and 7b display the SANS profiles for 10% (by mass fraction) over the temperature range 10 to 40 °C and 50 to 90 °C, respectively. The peak position shifts to substantially lower q values once the temperature is increased to 40 °C. The fit to a polydisperse hard sphere model (Fig. 7a inset—16% polydispersity, 50 Å radius) works well, and the presence of $S(q)$ becomes apparent at low q. The identification of such an ordered phase is difficult to distinguish from SANS alone since higher-order reflections are required to assign the geometry of the micellar packing. Since only one $S(q)$ reflection is present, we shall attribute such SANS spectrum to polydisperse weakly interacting spheres. As the temperature is increased to 50 °C, a second maximum in $P(q)$ is observed at 0.028 $Å^{-1}$ in addition to that from the polydisperse hard spheres (as observed at low temperatures). This is indicative of a second phase present, such as ellipsoidal micelles. This assumption proves consistent with the observations made at lower concentration, i.e., on increasing temperature the micelles elongate into ellipsoidal and worm-like structures. The inset in Fig. 7b shows the fit to a worm-like micelle for 90 °C. The fit parameters to this model are a contour length, L, of 2500 Å, a Kuhn length, b, of 100 Å (indicating a high degree of chain flexibility), and a radius, R, of 43 Å.

Fig. 8 shows the SANS profiles of 20 wt% polymer at various temperatures. At a temperature of 50 °C there is an obvious broadening of the peak characteristic of an order–disorder transition (ODT). However, the SANS intensity continues to increase due to increased fluctuations as the ODT is approached. At elevated temperatures, such as 90 °C, the peak is no longer evident indicating that the micelles are in a disordered array. The scaling of $I(q)$ at low q follows $q^{-1.6}$ at 90 °C, which is indicative of worm-like micelles, indicating that in the ordered state the micelles may pack into a hexagonal array. This, however, is an assumption since higher-order reflections are not defined clearly enough to confirm this; however, the fact that the peak arising from $S(q)$ contributions is sharper than that at 10% polymer (by mass fraction) implies that the micelles have stronger correlations with each other and the arrangement of micelles is becoming somewhat more ordered.

On increasing the block copolymer concentration to 40 wt%, a lyotropic liquid crystalline phase is observed over the whole temperature range, as seen in Fig. 9a. It is shown

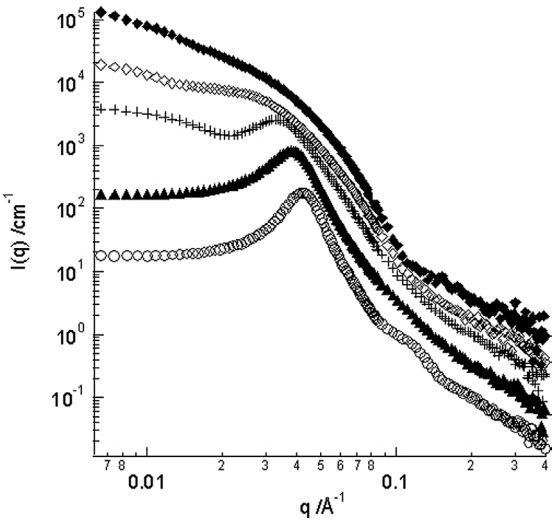

Fig. 8. SANS intensity profiles from a solution of 20% by mass fraction of $EO_{18}BO_9$ at various temperatures (open circles, 10 °C; filled triangles, 30 °C; crosses, 40 °C; open diamonds, 50 °C; filled diamonds, 90 °C).

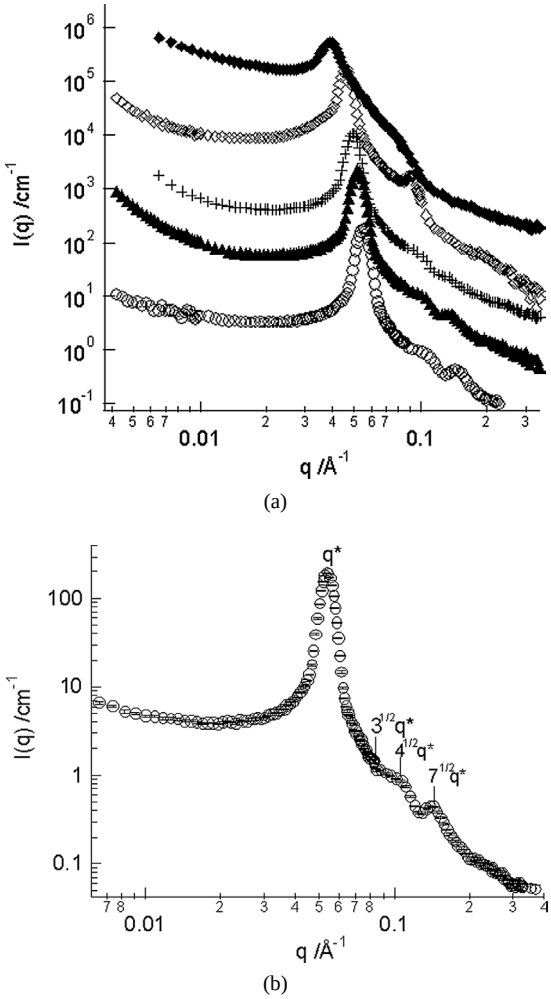

Fig. 9. (a) SANS intensity profiles from a solution of 40% by mass fraction of $EO_{18}BO_9$ at various temperatures (open circles, 10 °C; filled triangles, 30 °C; crosses, 40 °C; open diamonds, 50 °C; filled diamonds, 90 °C). (b) Expanded SANS profile for 40% by mass fraction $EO_{18}BO_9$ at 20 °C showing four orders of reflection indicative of hexagonally packed rod-like micelles.

that on increasing the temperature of the system, the domain spacing (or periodicity) is shown to increase (due to a shift in SANS peak to lower q values) suggesting that the micelles break apart from one another to a less densely packed arrangement. At lower temperatures a hexagonally packed micellar arrangement is favored as indicated by the ratio in peak positions relative to the first-order reflection. In addition, on heating, a hexagonal to lamellar phase transition is observed at approximately 40 °C where the peaks at $\sqrt{3}q^*$ and $\sqrt{7}q^*$ disappear and the peak at $\sqrt{4}^*$ intensifies.

The SANS profiles show orders of peaks that are in the ratio $1{:}\sqrt{3}{:}\sqrt{4}{:}\sqrt{7}$ at low temperature (20 °C) (see Fig. 9b) indicative of hexagonally packed rod-like micelles.

4. Discussion

The data and modeling undertaken in this work follow the work by Hamley et al. [21] and Soni et al. [18]. Our data covers a wider temperature and composition than the previous studies, and provides new analysis of $p(r)$ to characterize the elongation of the micelles. However, much of the work can be compared to works by Yu et al. [37], Hamley et al. [21], Chaibundit et al. [19,20], and Soni et al. [18].

In this work, the determination of the critical micelle concentration was not performed. Since this was previously reported by Soni et al. [18] (cmc = 0.0336 g/dm^3) and Yu et al. [37] (cmc = 0.035 g/dm^3) for the same polymer that we used (but of a different batch), it was decided that we would prepare concentrations of 0.2 wt% and over. This ensured we were working over the critical micelle concentration.

The characterization of the micelle sizes was performed by extracting parameters from the SANS models used. Yu et al. [37] and Chaibundit et al. [19] used dynamic light scattering to determine the hydrodynamic radius. We find that our results agree remarkably well with the data taken by Yu and Chaibundit. We find the radius of the spherical species to be of the order of 50–60 Å, depending on temperature and concentration. Soni et al. [18] use a different SANS model to extract a core radius of 43 Å and a hard sphere radius of 100 Å. The differences in radii between our and Soni's lead to pronounced differences in the aggregation number.

The aggregation number for spherical micelles that we determine is between 35 and 60 (see Table 2), depending on temperature. This shows fairly good agreement with data taken by Yu et al. [37] ($N = 70$ at 25 °C and $N = 110$ at 40 °C) and Chaibundit et al. [19] for $E_{11}B_8$ ($N = 63$ at 30 °C and $N = 334$ at 40 °C). We observe a rapid increase in N at 50 °C, where we measure $N = 334$ (0.2 wt% polymer). We attribute the differences we observe due to the solvent. We use deuterated water whereas Yu et al. [37] and Chaibundit et al. [19] used hydrogenated water. Using D_2O is known to (a) cause noticeable effects in phase transition temperatures and (b) result in ∼10% stronger hydrogen bonding

between polymer and solvent [38]. Considering such differences, and the fact that different batches were used on entirely different instruments, the comparison of our data to these previous experiments shows remarkable reproducibility. We would expect the value of N from Soni et al. [18] to be even more agreeable to our data since both measurements were performed using SANS. However, this is not the case. Soni et al. show much larger values of N than any other data previously reported: $N = 318$–340 at 30 °C and $N = 743$ at 50 °C. Whilst Soni describes this discrepancy in terms of technique—dynamic light scattering measures the hydrodynamic radius, R_h, and it is not trivial to obtain measurements of N from R_h since the degree of hydration is not known—we cannot ignore the fact that our data agrees extremely well with all other previously reported values of size and aggregation number. We attribute the differences in our data and the data recorded by Soni et al. in term of the modeling used to quantify our dimensions: Soni uses a structure factor in the modeling whereas we neglected this since we were only probing very low concentrations where inter-particle contributions are negligible. We determine N from Eq. (5) which utilizes $I(0)$. Since we used the 30 m SANS instrument at the NCNR [25], the q range we probe is much broader than that used by Soni et al. [18]. Hence, the values of $I(0)$ for each instrument are likely to be very different, which would result in very different values of N. The minimum q value shown in Soni's data is 0.02 Å^{-1}, corresponding to maximum dimensions of 314 Å, whereas our experiments probe to a much lower q range (allowing dimensions in excess of 1000 Å). Our larger q range has enabled the modeling of these worm-like micelles to extract the dimensions of their length, rather than assuming an ellipsoidal shape. However, both our data and the data recorded by Soni et al. [18] show that there is a rapid increase in N at approximately 50 °C corresponding to a change in micelle shape.

By referring to Table 2 it is shown that the radius of the spherical micelles increases up to a point. This point is between 40 and 50 °C, for the low concentrations of 0.2 and 1.0 wt% samples. After this point, the aggregation number rapidly increases (from 40 °C ($n_{agg} = 58$) to 50 °C ($n_{agg} = 334$)), which is indicative of a change in morphology of the micelles. This is coupled with the strong dependence on q of $I(q)$ in the low q region of the SANS curve. This was modeled and at 50 °C, the spherical model for the micelles no longer satisfies the data and either a prolate ellipsoid model or a model describing semi-flexible chains with excluded volume was used. Both models show elongation of the micelle, with dimensions increasing up to 1500 Å (1.0 wt% polymer at 90 °C). There is further evidence which suggests that such micelles are no longer spherical: The pair distance distribution function, shown as an inset to Fig. 6, is no longer symmetric about a mean particle radius. A sharp peak is observed with a roughly linear decrease to zero. This linear regime is due to the cylinder axis and the non-linearity is a result of the flexibility about the axis. This flexibility can be quantified by the ratio of the contour length, L, to the Kuhn length, b. At higher temperatures (90 °C for 1.0 wt%), this ratio is 15:1 compared to ∼8:1 for the polymer of 0.2 wt% at 50 °C. The reasoning behind such micelle elongation has been reported [21] and is due to dehydration of the micelle corona at higher temperatures: As the polymer solution is heated, the water (in our case D_2O) becomes a poorer solvent for the PEO corona, resulting in a reduced coverage of the PBO core by the PEO corona. This effect is more pronounced at shorter EO block lengths (and hence is not observed for block copolymers such as $E_{41}B_8$ [8]). This brings about an increase in the volume of the micelle core, however, such a process cannot continue indefinitely since this would lead to an overstretching of the micelle core. Hence, the micelle stretches outward to increase in volume and restore the stability. Such a mechanism leads to the formation of long, flexible, worm-like structures. A plausible intermediate for such a mechanism is postulated: The formation of prolate ellipsoid structures. These are shown in Table 2 for 1.0 wt% polymer, but not for 0.2 wt% polymer. We believe that this is because the formation of worm-like species is faster in the more dilute systems.

An interesting feature of the SANS profile at 1.0% is that at the very low q deviation from the typical SANS profile for a sphere was seen, which has been attributed to weak aggregation between the micelles [39]. The micelles are not packed into a geometric array since this would cause a diffraction peak at a higher q value. We postulate that the micelles remain in a disordered array but on a larger scale there is some correlation between the micelles, resulting in this sudden increase in scattered intensity. This is occurring at such a low q range that it may also be possible to study this phenomenon by small angle light scattering. It should be noted that, to the authors' knowledge, no such aggregation has previously been observed at such a low concentration for block copolymers of this architecture.

From Figs. 2–9 it is clear that on increasing polymer concentration there is a marked effect on the SANS profiles.

The main change is the appearance of a peak as the concentration increases. This tells us that the micelles have packed together into an ordered array. In some cases, higher-order peaks are observed allowing the identification of the lyotropic liquid crystalline phase.

Fig. 10 shows the effect of constant temperature and variation in concentration. All temperatures follow the same pattern, in that increasing the concentration induces lyotropic liquid crystal formation. As the concentration increases from 0.2 to 1.0% (by mass fraction), there is little change in the SANS profile in terms of shape. The shape of the SANS profile at low q indicates the existence of spherical micelles over this concentration range, at 20 °C, and is confirmed by the fit to the polydisperse hard sphere model. Increasing the concentration to 10.0% produces a pronounced change, resulting in a low intensity, broad peak at low q giving a periodicity of approximately 200 Å.

Table 3 summarizes all positions of q^* and the corresponding domain spacing over the concentration and temper-

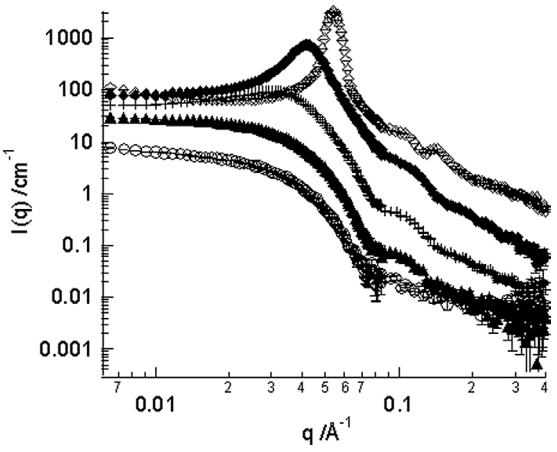

Fig. 10. SANS intensity profiles for $EO_{18}BO_9$ at 20 °C over a range of concentration (open circles, 0.2%; filled triangles, 1.0%; crosses, 10.0%; filled diamonds, 20.0%; open diamonds, 40.0% (all % by mass fraction)).

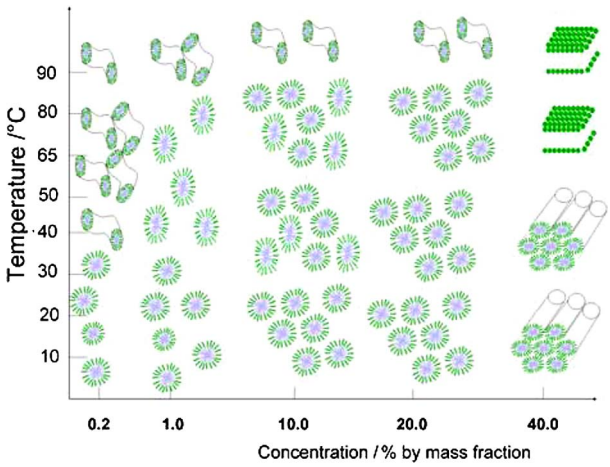

Fig. 11. Schematic describtion of the micelle shape and aggregation of $EO_{18}BO_9$ in D_2O with varying temperature and concentration.

Table 3
Principle peak position, domain size and peak ratio for a range of concentrations and temperatures of $EO_{18}BO_9$ in D_2O

Concentration (wt%)	Temperature (°C)	q^* ($Å^{-1}$)	d (Å)	Ratio of peak positions to q^*
10.0	10	0.03097	202.9	–
	20	0.03010	208.7	–
	30	0.02923	215.0	–
	40	0.02748	228.6	–
	50	0.02574	244.1	–
	65	0.02487	252.6	–
	80	0.02399	261.9	–
	90	Over B/S	–	–
20.0	10	0.04317	145.5	–
	20	0.04317	145.5	–
	30	0.03968	158.4	–
	40	0.03446	182.3	–
	50	0.02138	293.9	–
	65	Over B/S	–	–
	80	Over B/S	–	–
	90	Over B/S	–	–
40.0	10	0.05623	111.7	$1:\sqrt{3}:\sqrt{4}:\sqrt{7}$
	20	0.05449	115.3	$1:\sqrt{3}:\sqrt{4}:\sqrt{7}$
	30	0.05275	119.1	$1:\sqrt{3}:\sqrt{4}:\sqrt{7}$
	40	0.05014	125.3	$1:\sqrt{4}$
	50	0.04665	134.7	$1:\sqrt{4}$
	65	0.04143	151.7	$1:\sqrt{4}$
	80	0.04056	154.9	–
	90	0.03881	161.9	–

ature range of interacting systems. The SANS data at 20.0% shows that the domain spacing decreases to 146 Å due to the shift of the peak to higher q values. This trend is also evident as the concentration reaches 40.0%, where the domain spacing becomes 112 Å. In addition, three higher orders of reflection are observed, as shown in Fig. 9b where hexagonal arrays of cylindrical micelles are present. At higher temperatures, worm-like micelles were detected by SANS at low concentration to form the hexagonal phase. The effect of concentration is the same here; the micelles pack closer until an ordered phase is reached, and as they do this the domain spacing decreases and higher orders of reflection are observed. At temperatures over 40 °C, the lyotropic liquid crystalline phase that forms at higher concentrations is the lamellar phase, agreeing with previous studies [7,8,40–45] which show the cubic to hexagonal to lamellar phase transition as the temperature is increased for similar block copolymers.

Fig. 11 provides a schematic illustrating the changes in micelle shape and micelle aggregation as a function of temperature and concentration.

5. Conclusions

SANS experiments reveal the transition from spherical micelles to worm-like micelles at low concentration for the diblock copolymer $E_{18}B_9$. A fit to the polydisperse hard sphere works well for the low concentration. The upturn in scattered intensity at low q, scaling as $q^{-1.63}$, predicts that the worm-like micelles are in existence at higher temperatures, agreeing with works by Hamley et al. [21] and Soni et al. [18]. This was proved by the fit to the appropriate model, the determination of the aggregation number from $I(0)$, and the resulting $p(r)$ function analysis. The change in slope is not dramatic and scalings as $q^{-0.5}$ and q^{-1} are observed, which may indicate ellipsoidal and rigid rod shapes for the micelles. The reasoning behind this observation is the dehydration of the polar ethylene oxide corona at elevated temperatures and is dependent on the E block length. The calculation of the $p(r)$ using an indirect Fourier transformation provides further evidence for the elongation and flexibility of these micelles.

The consequence of such micelle elongation on the lyotropic nature of the block copolymer at higher concentrations is to form gel networks of hexagonally packed cylinders. Such structures are observed at 40 wt% and undergo a thermally induced cylindrical to lamellar phase transition.

References

[1] I.W. Hamley, The Physics of Block Copolymers, Oxford Univ. Press, Oxford, UK, 1998.
[2] V.M. Nace, Non-Ionic Surfactants—Poly(oxyalkylene) Block Copolymers, Surfactant Series, vol. 60, Dekker, New York, 1996.
[3] I.W. Hamley, Introduction to Soft Matter—Polymers, Colloids, Amphiphiles, and Liquid Crystals, Wiley, Chichester, 2000.
[4] C. Booth, D. Attwood, Macromol. Rapid Commun. 21 (2000) 501.
[5] L.G. Lundsted, British 722.746, Wyandotte Chemicals Corp., 1955.
[6] B-Series Polyglycols, Butylene Oxide/Ethylene Oxide Block Copolymers, Product Brochure, The Dow Chemical Co., Freeport, TX, 1992.
[7] G.-E. Yu, H. Li, J.P.A. Fairclough, A.J. Ryan, N. McKeown, Z. Ali-Adib, C. Price, C. Booth, Langmuir 14 (1998) 5782.
[8] J.P.A. Fairclough, A.J. Ryan, I.W. Hamley, H. Li, G.-E. Yu, C. Booth, Macromolecules 32 (1999) 2058.
[9] A.I. Norman, J.P.A. Fairclough, S. Mai, A.J. Ryan, J. Macromol. Sci. Phys. 43 (2004) 71.
[10] J.A. Pople, I.W. Hamley, J.P.A. Fairclough, A.J. Ryan, B.U. Komanschek, A.J. Gleeson, G.-E. Yu, C. Booth, Macromolecules 30 (1997) 5721.
[11] I.W. Hamley, J.A. Pople, J.P.A. Fairclough, N.J. Terrill, A.J. Ryan, C. Booth, G.-E. Yu, O. Diat, K. Almdal, K. Mortensen, M. Vigild, J. Chem. Phys. 108 (1998) 6929.
[12] I.W. Hamley, J.A. Pople, J.P.A. Fairclough, A.J. Ryan, C. Booth, Y.W. Yang, Macromolecules 31 (1998) 3906.
[13] A. Kelarakis, V. Castelletto, C. Chaibundit, J. Fundin, V. Havredaki, I.W. Hamley, C. Booth, Langmuir 17 (2001) 4232.
[14] J.N. Israelachvili, D.J. Mitchell, B.W. Ninham, J. Chem. Soc. Faraday Trans. 2 72 (1976) 1525.
[15] S.M. King, R.K. Heenan, V.M. Cloke, C. Washington, Macromolecules 30 (1997) 6215.
[16] K. Mortensen, J.S. Pedersen, Macromolecules 26 (1993) 805.
[17] K. Mortensen, W. Brown, Macromolecules 26 (1993) 4128.
[18] S.S. Soni, N.V. Sastry, A.K. Patra, J.V. Joshi, P.S. Goyal, J. Phys. Chem. B 106 (2002) 13069.
[19] C. Chaibundit, N.M.P.S. Ricardo, H. Crothers, C. Booth, Langmuir 18 (2002) 4277.
[20] C. Chaibundit, P. Sumanatrakool, S. Chinchew, P. Kanatharana, C.E. Tattershall, C. Booth, X.-F. Yuan, J. Colloid Interface Sci. (2005), in press.
[21] I.W. Hamley, J.S. Pedersen, C. Booth, V.M. Nace, Langmuir 17 (2001) 6386.
[22] J.A. Pople, I.W. Hamley, J.P.A. Fairclough, A.J. Ryan, C. Booth, Macromolecules 31 (1998) 2952.
[23] J.K. Harris, G.D. Rose, M.L. Bruening, Langmuir 18 (2002) 5337.
[24] A.A. Riberio, E.A. Dennis, in: M.J. Shick (Ed.), Nonionic Surfactants: Physical Chemistry, Dekker, New York, 1987, pp. 975–979.
[25] C.J. Glinka, J.G. Barker, B. Hammouda, S. Krueger, J.J. Moyer, W.J. Orts, J. Appl. Cryst. 31 (1998) 430.
[26] S.-M. Choi, J.G. Barker, C.J. Glinka, Y.-T. Cheng, P.L. Gammel, J. Appl. Cryst. 33 (2000) 793.
[27] J. Lemmich, K. Mortensen, J.H. Ipsen, T. Honger, R. Bauer, O.G. Mouritsen, Phys. Rev. E 53 (1996) 5169.
[28] A. Guinier, G. Fournet, Small Angle Scattering of X-Rays, Wiley, New York, 1955.
[29] G. Porod, in: O. Glatter, O. Kratky (Eds.), Small Angle X-Ray Scattering, Academic Press, London, 1982.
[30] G. Beaucage, J. Appl. Cryst. 28 (1995) 717.
[31] O. Glatter, in: P. Lindner, T. Zemb (Eds.), Neutrons, X-Rays, and Light: Scattering Methods Applied to Soft Condensed Matter, Elsevier, 2000.
[32] O. Glatter, J. Appl. Cryst. 10 (1977) 415.
[33] O. Glatter, J. Appl. Cryst. 13 (1980) 577.
[34] W.L. Griffith, R. Triolio, A.L. Compere, Phys. Rev. A 35 (1987) 2200.
[35] http://www.ncnr.nist.gov/resurces/sansmodels.
[36] J.S. Pedersen, P. Schurtenberger, Macromolecules 29 (1996) 7602.
[37] G.E. Yu, Y.W. Yang, Z. Zhang, D. Attwood, C. Booth, Langmuir 12 (1996) 3404.
[38] A. Engdahl, B. Nelander, J. Chem. Phys. 86 (1987) 1819.
[39] A.-M. Hecht, F. Horkay, E. Geissler, J. Phys. Chem. B 105 (2001) 5637.
[40] L. Derici, S. Ledger, S. Mai, C. Booth, I.W. Hamley, J.S. Pedersen, Phys. Chem. Chem. Phys. 1 (1999) 2773.
[41] Y. Deng, R.N. Young, A.J. Ryan, J.P.A. Fairclough, A.I. Norman, R.D. Tack, Polymer 43 (2002) 7155.
[42] H. Li, G.-E. Yu, C. Price, C. Booth, J.P.A. Fairclough, A.J. Ryan, K. Mortensen, Langmuir 19 (2003) 1075.
[43] H. Li, G.-E. Yu, C. Price, C. Booth, E. Hecht, H. Hoffmann, Macromolecules 30 (1997) 1347.
[44] I.W. Hamley, S. Mai, A.J. Ryan, J.P.A. Fairclough, C. Booth, Phys. Chem. Chem. Phys. 3 (2001) 2972.
[45] J.P.A. Fairclough, I.W. Hamley, N.J. Terrill, Rad. Phys. Chem. 56 (1999) 159.